Nuclear Engineering and Technology 54 (2022) 386–400

Contents lists available at ScienceDirect

Nuclear Engineering and Technology

journal homepage: www.elsevier.com/locate/net

Original article

Seismic performance assessment of NPP concrete containments considering recent ground motions in South Korea

Chanyoung Kim [a], Eun Jeong Cha [b], Myoungsu Shin [a, *]

[a] Dept. of Urban and Environmental Engineering, Ulsan National Institute of Science and Technology (UNIST), Ulsan, 44919, South Korea
[b] Dept. of Civil and Environmental Engineering, University of Illinois at Urbana-Champaign, Urbana, IL, USA

ARTICLE INFO

Article history:
Received 8 April 2021
Received in revised form
29 June 2021
Accepted 21 July 2021
Available online 22 July 2021

Keywords:
NPP concrete Containment
Seismic probabilistic risk assessment
Seismic fragility analysis
Spectral-matched time history
Earthquake characteristics

ABSTRACT

Seismic fragility analysis, a part of seismic probabilistic risk assessment (SPRA), is commonly used to establish the relationship between a representative property of earthquakes and the failure probability of a structure, component, or system. Current guidelines on the SPRA of nuclear power plants (NPPs) used worldwide mainly reflect the earthquake characteristics of the western United States. However, different earthquake characteristics may have a significant impact on the seismic fragility of a structure. Given the concern, this study aimed to investigate the effects of earthquake characteristics on the seismic fragility of concrete containments housing the OPR-1000 reactor. Earthquake time histories were created from 30 ground motions (including those of the 2016 Gyeongju earthquake) by spectral matching to the site-specific response spectrum of Hanbit nuclear power plants in South Korea. Fragility curves of the containment structure were determined under the linear response history analysis using a lumped-mass stick model and 30 ground motions, and were compared in terms of earthquake characteristics. The results showed that the median capacity and high confidence of low probability of failure (HCLPF) tended to highly depend on the sustained maximum acceleration (SMA), and increase when using the time histories which have lower SMA compared with the others.

1. Introduction

Nuclear power plants (NPPs) are one of the primary energy-producing facilities in modern society. NPPs include structures, systems, and components that pose a potential extreme hazard to the environment, leading to strict safety requirements for a much lower probability of failure compared with conventional facilities [1–3]. Several methodologies have been proposed since the 1970s to evaluate the safety of NPPs and to prevent possible accident scenarios [4]. Early plant examination programs conducted in the U.S. investigated the contribution of seismic events to the core damage risk of NPPs. During this period, the lognormal fragility model was developed to define the capacity of a plant, and is still used in current assessments [5–7]. In the 1990s, seismic probabilistic risk assessments (SPRAs) and seismic margin assessments were widely used to evaluate the safety of NPPs due to seismic events [8]. Among these, SPRAs focus on the variabilities in the seismic input, structure response, and material properties [8–10]. After 2000, the updates on the TR-103959 guidelines or reports including new observations have been suggested by Electric Power Research Institute (EPRI) [11–14]. The EPRI 1019200 [12] include the several updates to the logarithmic standard deviation of basic variables due to the peak-to-valley variability in TR-103959 [8]. The EPRI-3002004396 suggest the guidance for the seismic probabilistic risk assessment, considering the potential high frequency effects on the seismic fragility of components [14]. Furthermore, several studies have been proposed to conduct the SPRA for the multi-unit NPP [15–17] and to improve the methodologies for seismic fragility analysis [18].

The methodology suggested by the U.S. Nuclear Regulatory Commission (NRC), which has been widely used in seismic performance assessments, is based on the response spectra that were developed through studies on earthquake records in the western U.S [7,11,12]. Therefore, when this assessment is used in other countries, the shape of the response spectra should be modified to fit well with the characteristics of local ground motion. Furthermore, appropriate time histories of ground motion should be chosen for a better assessment [18–23]. Several previous studies have investigated the effects of earthquake characteristics on the

* Corresponding author.
E-mail address: msshin@unist.ac.kr (M. Shin).

https://doi.org/10.1016/j.net.2021.07.035

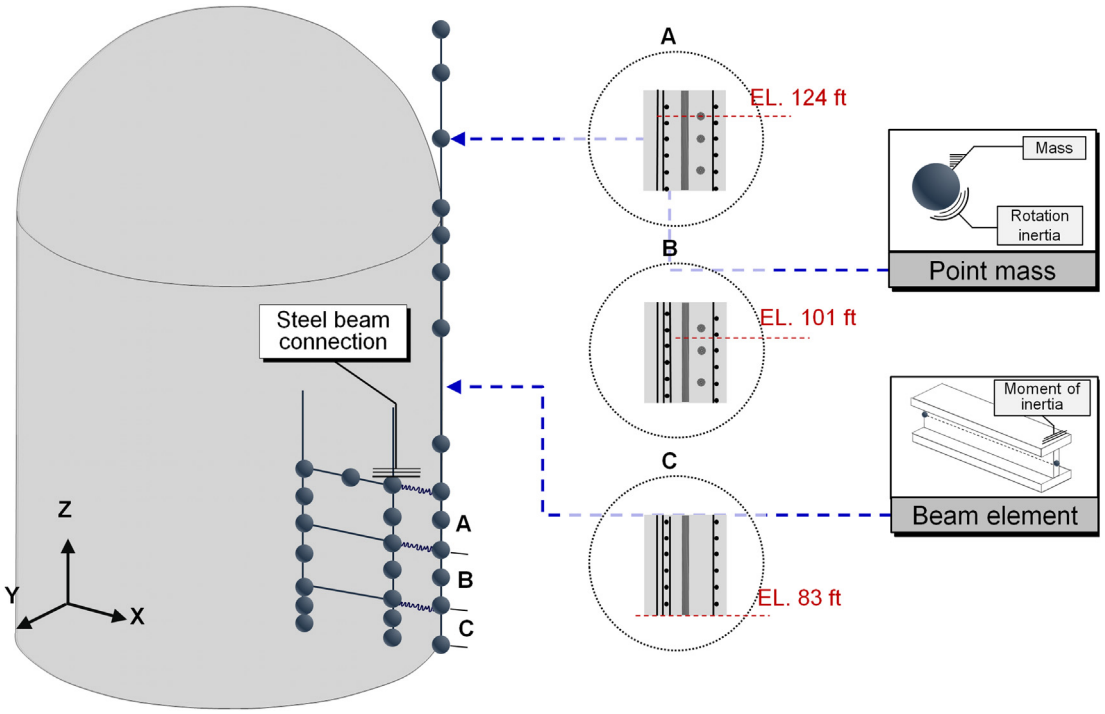

Fig. 1. Schematic elevation view of the OPR-1000 reactor containment structure.

Table 1
Design details for the OPR-1000 containment structure; adapted from Lee and Song [34].

Elevation (ft)		83 (C in Fig. 1)	101 (B in Fig. 1)	124 (A in Fig. 1)
Reinforcing steel ratio	Meridional	1.70 %	1.23 %	0.645 %
	Hoop	0.78 %	0.78 %	0.78 %
Prestressing steel ratio	Meridional	0.60 %	0.60 %	0.60 %
	Hoop	0	0.98 %	0.98 %
Material properties used in the design of structure		Concrete elastic modulus		609000 ksf
		Concrete compressive strength		5500 psi (at 91 days)
		Reinforcement yield strength		60000 psi
		Prestressing steel yield strength		229500 psi
		Damping ratio		7 % (median)
				5 % (design)

Table 2
Information for natural frequency and effective mass ratio of lumped mass model (containment wall).

Mode information	Natural frequency (Hz)	Effective mass ratio (%)
Translational in X-direction – mode 1	4.6411	60.52
Translational in Y-direction – mode 1	4.6564	61.17
Translational in X-direction – mode 2	13.972	22.82
Translational in Y-direction – mode 2	14.030	22.91
Translational in X-direction – mode 3	20.249	2.38
Translational in Y-direction – mode 3	20.280	1.92

cumulative damage of structures [24–27]. In general, the peak ground acceleration (PGA), peak ground velocity (PGV), peak ground displacement (PGD), and spectral acceleration (S_a) are used as intensity measures for the development of seismic fragility curves [18–29]. Meanwhile, there is a recent study suggested that the sustained maximum acceleration (SMA) can be used as an intensity measure for estimating the seismic demand on structures in limited cases [30]. Therefore, the earthquake characteristics of ground motions, such as the peak ground acceleration (PGA), peak ground velocity (PGV), peak ground displacement (PGD), spectral acceleration (S_a), and sustained maximum acceleration (SMA) should be considered simultaneously [28–30].

In this study, seismic fragility analyses on the reinforced concrete containment of an OPR-1000 reactor NPP were performed using 30 ground motion data recorded around the world. In particular, ground motion records of the Gyeongju earthquake in 2016 were considered, along with other records obtained from the database of Pacific Earthquake Engineering Research Center (PEER) [31,32]. Earthquake time histories were created from the selected ground motions by spectral matching to the site-specific response

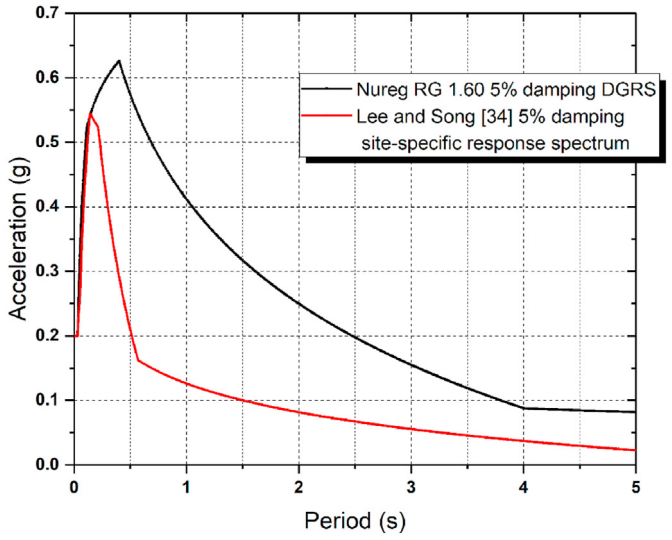

Fig. 2. Design response spectrum (DGRS) and site-specific response spectrum [4,8,34].

spectrum of Hanbit nuclear power plants in South Korea. Linear response history analyses were conducted using a lumped-mass stick model to estimate the response of the considered structure. The effects of ground motions on the seismic fragility of the structure were analyzed in terms of significant duration, Arias intensity, root mean square of acceleration (acceleration RMS), characteristic intensity, and sustained maximum acceleration (SMA). Finally, considerations when using the earthquake records for the seismic performance assessment of NPP concrete containments were discussed.

2. Target structure and numerical model

The structure considered in this study is OPR-1000 NPP, a two-loop 1000 MWe PWR Generation II nuclear reactor developed by Korea Hydro & Nuclear Power Co., Ltd. (KHNP) and Korea Electric Power Corporation (KEPCO) in South Korea [33]. The concrete containment structure is composed of two layers of deformed bars and tendons in the concrete wall and dome, as well as a steel liner, as shown in Fig. 1 and Table 1. This structure exhibits a continuity between its cylindrical wall and dome. The wall and dome have three buttresses with equal angles; therefore, hoop tendons at each elevation extend to 240°. The reinforcement ratio in the containment wall near the base is approximately 1.70 % in the meridional direction and 0.78 % in the hoop direction, while the reinforcement ratio at the spring line of the wall is approximately 0.65 % in the meridional direction and 1.39 % in the hoop direction [34]. In addition, the prestressing steel ratio at the part near the base is approximately 0.60 % in the meridional direction and absent in the hoop direction, while the reinforcement ratio at the spring line of the wall is approximately 0.60 % in the meridional direction and 0.98 % in the hoop direction.

As the containment structure generally behaves as a cantilever beam when subjected to earthquake ground motion, many past studies and several recent studies have simplified the containment structure as a lumped mass model which consists of lumped masses at nodes and beam elements, as depicted in Fig. 1 [27,30,34–41]. In addition, lumped mass models successfully estimate the seismic base shear of containment structures in elastic region in recent studies [27,30,39–41]. In this study, the ABAQUS software was used to construct the lumped mass model. The beam element was defined by assigning a generalized profile with an area, moment of inertia, Young's modulus, and shear modulus to enable the beam to exhibit proper values of bending and shear

Table 3
Selected ground motion data [31,32].

No.	Earthquake name	Station name	Year	M_w	R_{rup} orR_{epic}[a] (km)	PGA (g)	Maximum misfit (%)[b]
1	Parkfield	Shandon Array #8	1966	6.19	12.90	0.125	14.67
2	San Fernando	Santa Felita Dam 172	1971	6.61	24.87	0.155	20.56
3	San Fernando	Santa Felita Dam 262	1971	6.61	24.87	0.155	11.62
4	Imperial Valley	Cerro Prieto 147	1979	6.53	15.19	0.168	9.62
5	Irpinia, Italy	Brienza	1980	6.90	22.56	0.220	13.65
6	Irpinia, Italy	Rionero In Vulture	1980	6.20	22.69	0.100	11.40
7	Coalinga-01	Parkfield – Fault Zone 16	1983	6.36	27.67	0.183	12.49
8	Morgan Hill	Gilroy Array #4270	1984	6.19	11.54	0.224	18.18
9	Chalfant Valley	Benton 270	1986	6.19	21.92	0.209	8.734
10	Loma Prieta	Coyote Lake Dam (Downst)	1989	6.93	20.80	0.160	13.39
11	Hector Mine	Hector	1999	7.13	11.66	0.265	23.03
12	El Mayor-Cucapah	Bond Corner	2010	7.20	32.85	0.192	28.88
13	Joshua Tree	Thousand Palms Post office	1992	6.10	17.86	0.229	15.99
14	Christchurch	Canterbury Aero Club	2011	6.20	14.41	0.184	14.80
15	Imperial Valley	USGS 5115	1979	6.40	31.00	0.315	26.50
16	Kobe	KAKOGAWA	1995	6.90	22.50	0.345	22.19
17	Northridge	Castaic – Old Ridge Route	1994	6.69	20.72	0.568	25.13
18	Gyeongju	HDB	2016	5.80	19.33	0.056	8.162
19	Gyeongju	DAG2	2016	5.80	26.28	0.062	6.93
20	Gyeongju	PHA2	2016	5.80	50.83	0.028	12.77
21	Gyeongju	GKP1	2016	5.80	54.42	0.046	16.09
22	Gyeongju	BUS2	2016	5.80	57.45	0.062	25.03
23	Gyeongju	ADO2	2016	5.80	75.60	0.044	19.03
24	Gyeongju	ULJ2	2016	5.80	106.6	0.008	23.28
25	Gyeongju	GSU	2016	5.80	119.7	0.005	18.09
26	Gyeongju	TOY	2016	5.80	122.7	0.022	10.12
27	Gyeongju	UJN	2016	5.80	138.5	0.066	12.81
28	Gyeongju	SND	2016	5.80	159.4	0.003	22.68
29	Gyeongju	CHR	2016	5.80	67.40	0.069	10.48
30	Gyeongju	DKJ	2016	5.80	21.87	0.092	11.02

[a] R_{rup} for PEER records, R_{epic} for Gyeongju earthquake records.
[b] Only in 2–10 Hz of frequency range.

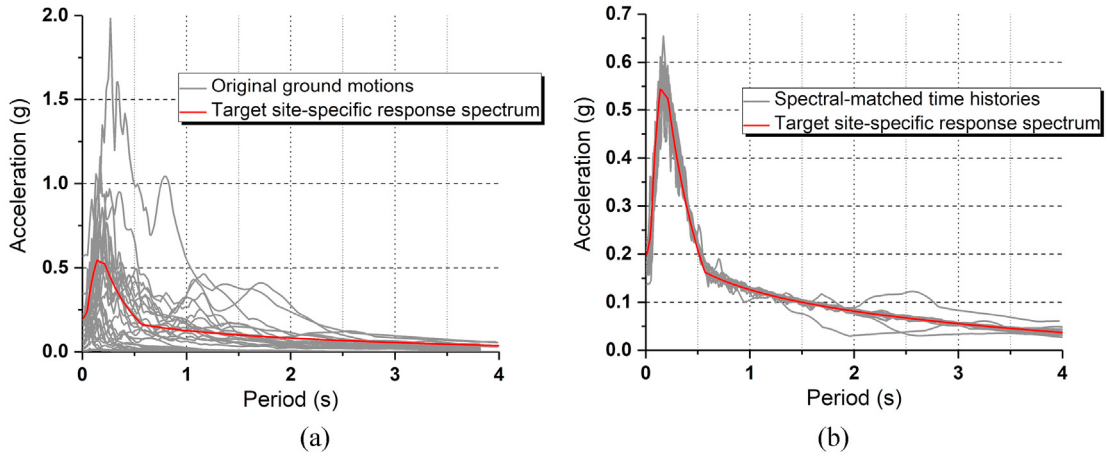

Fig. 3. Response spectra of original ground motions (a) and spectral-matched time histories (b) [34].

Table 4
Characteristics of earthquake time histories spectral-matched to the site-specific response spectrum.

No. of original ground motion	PGA (g)	$(S_a)_n$(g)[1)]	Significant duration (s)	Arias intensity	Acceleration RMS (g)	Characteristic intensity	SMA (g)
1	0.1584	0.5429	11.2	0.2662	0.02568	0.02106	0.1243
2	0.1597	0.5348	22.04	0.2761	0.02445	0.02093	0.1240
3	0.2009	0.4862	18.84	0.2766	0.02447	0.02096	0.1543
4	0.1595	0.5252	16.765	0.6439	0.03734	0.03950	0.1557
5	0.1646	0.5063	10.498	0.3550	0.03057	0.02654	0.1483
6	0.1769	0.5211	16.6286	0.3296	0.02946	0.02510	0.1389
7	0.2068	0.5430	12.64	0.2933	0.02521	0.02190	0.1207
8	0.1647	0.5348	14.5	0.3531	0.02765	0.02517	0.1517
9	0.1820	0.5064	16.645	0.2860	0.02488	0.02149	0.1288
10	0.1710	0.4990	14.005	0.3300	0.02673	0.02393	0.1354
11	0.1860	0.5325	13.35	0.4786	0.02869	0.02985	0.1605
12	0.1677	0.5254	21.4	0.6918	0.03669	0.04059	0.1545
13	0.2078	0.5141	11.16	0.4427	0.03217	0.03040	0.1641
14	0.1677	0.5032	12.93	0.3011	0.02407	0.02169	0.1589
15	0.1848	0.5176	13.6	0.5421	0.03459	0.03488	0.1638
16	0.1920	0.5277	11.95	0.7225	0.04839	0.04758	0.1715
17	0.2316	0.5010	18.66	0.5901	0.03573	0.03699	0.1799
18	0.2147	0.5121	1.600	0.1573	0.01772	0.01345	0.1564
19	0.1835	0.5139	4.950	0.1482	0.01635	0.01254	0.1429
20	0.1556	0.519	4.150	0.1446	0.01626	0.01236	0.1442
21	0.2261	0.5463	6.920	0.2106	0.01850	0.01590	0.1140
22	0.2153	0.5267	5.860	0.1586	0.01681	0.01316	0.1274
23	0.1632	0.5333	6.910	0.1797	0.01725	0.01418	0.1080
24	0.2324	0.5214	3.120	0.1453	0.01537	0.01204	0.1024
25	0.1362	0.5418	3.740	0.1715	0.01669	0.01363	0.0955
26	0.1828	0.5102	7.170	0.1973	0.01790	0.01514	0.1145
27	0.1738	0.5209	7.030	0.1802	0.01711	0.01415	0.0848
28	0.1702	0.4648	4.390	0.1507	0.01565	0.01237	0.0854
29	0.1810	0.5209	8.230	0.2146	0.01867	0.01613	0.1517
30	0.2245	0.5153	4.710	0.1388	0.01594	0.01199	0.0907
Median	0.1815	0.5209	11.18	0.2763	0.02446	0.0210	0.1409
COV	0.1345	0.0334	0.5200	0.5485	0.3340	0.4365	0.1934

[1)] Spectral acceleration (5% damping ratio) at the 1st natural frequency of the containment structure 4.64 Hz.

stiffness. Anisotropic masses were assigned in the model to independently analyze the behavior of the structure loaded by horizontal and vertical ground motions. The steel beam connection between containment building and internal structure was simplified by using beam element since this connection restrained the vertical displacements. The information for natural frequencies and effective mass ratios of first, second, and third modes of the containment structure is summarized in Table 2. It was assumed that safe shutdown earthquake (SSE)-levels of approximately 0.2 g PGA, which are used in seismic performance assessments of NPP structures, cause linear elastic behavior of the containment structure [7,8,11,12]. Therefore, the entire model was built using linear elastic elements, and the effects of nonlinear behavior that could be induced at a higher ground motion level compared with SSE was evaluated using the inelastic energy absorption factor. Rayleigh damping corresponding to 7 % or 5 % of critical damping was assigned to the structure to take into account the damping uncertainty (Table 1). Fixed time increments of 0.01 s, 0.005 s, or 0.0029 s to consider input ground motion were adopted for implicit dynamic analysis. For simplification, the lumped mass models excluded equipment such as the steam generator and heat exchanger. Also, the effects of soil structure interaction are excluded in this study due to the fact that the target structure is constructed to a hard rock site.

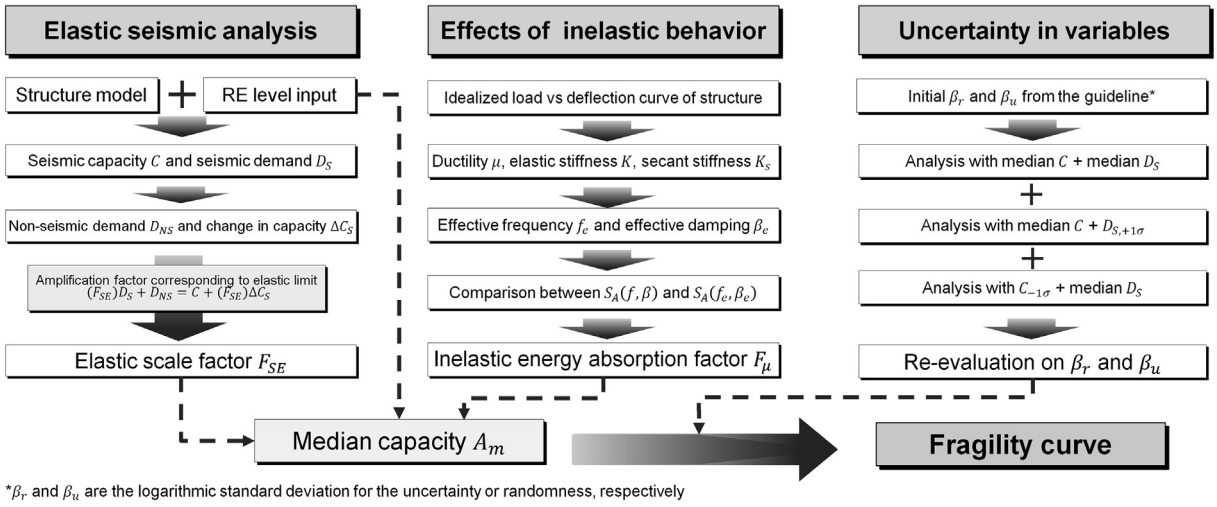

Fig. 4. Determination of fragility analysis parameters.

3. Ground motions

3.1. Target response spectrum

In the seismic fragility analysis of NPPs, appropriate time histories that satisfy TR-103959 published by Electric Power Research Institute (EPRI) are required. Spectrum matching with the response spectra is one of the available methods that can be used to develop proper time histories [4–8,11,12]. In general, the design response spectrum suggested in the U.S. NRC Regulatory Guide 1.60 (NUREG RG 1.60) is assumed to have a non-exceedance ratio of 84 % and is typically used in seismic margin assessment [4,8,11,12]. In contrast, the site-specific response spectrum is required to perform a seismic fragility analysis based on the separation of variables (SOV) method, and it is assumed that the site-specific response spectrum is constructed with the median value [34]. In addition, this study aimed at conducting the seismic performance assessment of Hanbit nuclear power plants in South Korea and investigating the effects of ground motion characteristics on the fragility curves. Therefore, it is appropriate to conduct spectral matching to site-specific response spectrum to compare the effects of ground motion characteristics of various earthquakes, including the ground motion records from Gyeongju earthquake. For this reason, earthquake time histories were generated by spectral matching to the 5 % damped site-specific response spectrum acquired following the study by Lee and Song [34]. The spectral matching has been conducted by following the guideline of NUREG-0800 [42]. The site-specific response spectrum for Hanbit 5 & 6 unit used in this study is depicted in Fig. 2 and is compared with the design response spectrum suggested in NUREG RG 1.60.

3.2. Ground motion selection

The ground motion records were selected from the PEER NGA West 2 ground motion database and the Korean Meteorological Administration (KMA) using the following criteria [31,32]. First, the ground motion records for earthquakes with magnitudes higher than 6.0 were obtained from the PEER database for comparison with the Gyeongju earthquake records. Thereafter, spectral matching processes were conducted to the selected ground motion with 40 iterations using SeismoMatch software. The misfit of spectral acceleration in the 2–10 Hz frequency range was limited to 30 %, by referring to the second approach suggested by Chapter 3 of NUREG-0800 [42]. Finally, the ground motion data that were well anchored to the site-specific response spectrum in the frequency range of 2–10 Hz were chosen. The information summarized in Table 3 contains the location, magnitude, rupture distance or epicenter distance, PGA, and misfit value for a total of 30 pairs of ground motion records. Significant differences in the PGA interval value and the epicenter distance exist between the selected Gyeongju earthquake records and the selected PEER records. Ground motion No. 28 recorded far from the epicenter shows a relatively lower PGA value among the selected earthquakes. However, it is consistent with the site-specific response spectrum in terms of the maximum misfit ratio. The response spectra of the original time histories and spectral-matched histories for selected ground motion are shown in Fig. 3(a) and Fig. 3(b), respectively. It is clear that the response spectra of the spectral-matched time histories were well matched with the target site-specific response spectrum.

3.3. Earthquake characteristics

Table 4 summarizes the earthquake characteristics of the produced ground motion, including PGA, spectral acceleration at the natural frequency of the containment structure $(S_a)_n$, significant duration, Arias intensity, acceleration RMS, characteristic intensity, and SMA. The first natural frequency of the containment structure was estimated to be 4.64 Hz (Table 2), which was similar to the reported value of 4.6 Hz in the literature [34]. The time histories developed in this study have similarity with each other in the PGA value and $(S_a)_n$ with the low coefficient of variations (COV). However, they show larger differences in significant duration, Arias intensity, acceleration RMS, characteristic intensity in terms of the COV. The significant durations of the time histories from Gyeongju earthquakes are comparatively shorter than those of the other time histories used in this study or the previous studies that dealt with the effects of ground motion duration on structural response [25,26,30,43–45]. Also, the difference in significant duration seems to be related with the differences in other ground motion parameters such as the Arias intensity, acceleration RMS and characteristic intensity as these parameters are defined in the time domain and the significant duration is the time interval that accounts for the distribution of seismic energy [46,47].

Furthermore, recent study has suggested that SMA is the intensity measure that can properly estimate the seismic demand in

limited cases. Nguyen et al. [30] discussed that SMA show strong correlation with the drift of containment structure when the near-fault ground motions were used for assessment. These indicate that using the time histories with lower SMA probably resulted in less seismic demand compared to other time histories. In this reason, comparative analysis was performed between the time histories to investigate the difference in structural response and seismic fragility parameters in section 5.

4. Seismic fragility analysis procedure

The seismic fragility analysis performed in this study is based on the method recommended in EPRI TR-103959 [8]. In this method, the limit state is defined as the operational failure of the structure, component, or system, and the seismic capacity is defined as the ability to resist seismic load in each failure mode. Seismic capacity can be expressed using the specific damage index such as stress, displacement, and acceleration. In this study, the occurrence of maximum tangential shear of the concrete containment structures is considered as the performance level for the fragility curves, and the corresponding damage index is the tangential shear stress [8,11,12]. Therefore, the ground motion level inducing elastic limit state of the structure, component, and system could be estimated using the elastic scale factor which considering the elastic behavior of containment structure. In addition, the effects of inelastic behavior are considered by using inelastic energy absorption factor. Moreover, the variabilities in basic variables are considered to estimate the probability of failure at varying PGA level from the median capacity of the structure. As a result, the fragility curve is constructed as a logarithmic standard distribution with several factors that consider the elastic limit of the structure, the inelastic behavior of the structure, and the uncertainties in seismic demand and seismic capacity. The flowchart for obtaining the main seismic fragility analysis parameters is shown in Fig. 4.

4.1. Failure mode and strength equation

In general, the tangential shear failure of the cylindrical wall near the base is considered as the governing failure mode of the containment structure subjected to ground motion [8,11,12,48]. This consideration is based on previous experimental studies on the structural behavior of small-scale reinforced and prestressed cylindrical walls subjected to horizontal loadings [49–53]. The failure of the containment wall observed in these previous studies proceeded in the following sequence: initiation of crack at the flange, propagation of crack to the web, and finally yielding of the vertical reinforcement at the web typically in the vertical direction. Several studies successfully estimate the shear stress at failure by using a concept known as the averaged reinforcement ratio [51,53]. The shear strength capacity equation suggested by Ogaki et al. [51] considered the abovementioned observations.

Therefore, the equation for the shear strength capacity of the containment structure suggested by Ogaki et al. [51] was applied in this study and is given by:

$$V_U = \frac{v_U \cdot \pi \cdot D_c \cdot t_w}{\alpha} \tag{1}$$

where V_U is the ultimate shear strength, v_U is the ultimate shear stress, D_c is the centerline diameter of the containment wall, t_w is the depth of the wall, and α is the coefficient of conversion.

In (1), the conversion coefficient α is used to evaluate the effects of the overturning moment on the shear resistance of structures. Coefficient α can be described by the following equations:

$$\begin{aligned} \alpha &= 2.0 && \text{for } \tfrac{M}{VD_0} \le 0.5 \\ \alpha &= 0.667\left(\frac{M}{VD_0}\right) + 1.67 && \text{for } 0.5 < \frac{M}{VD_0} < 1.25 \\ \alpha &= 2.5 && \text{for } 1.25 \le \frac{M}{VD_0} \end{aligned} \tag{2}$$

where M is the overturning moment, V is the shear force, and D_0 is the outer diameter of the containment wall structure.

The ultimate shear stress v_U is expressed as:

$$v_U = 0.8\sqrt{f_c} + (\rho\sigma_y)_{avg} < 21.1\sqrt{f_c} \tag{3}$$

where f_c is the compressive strength of concrete at 28 days of curing (psi) and $(\rho\sigma_y)_{avg}$ is the averaged reinforcement ratio expressed by (4):

$$(\rho\sigma_y)_{avg} = \frac{(\rho_h + \rho_m)}{2} f_y + \frac{\left(\rho_{ph} + \rho_{pm}\right)}{2} f_{py} - \frac{(\sigma_h + \sigma_m)}{2} \tag{4}$$

where ρ_h is the reinforcement ratio in the hoop direction, ρ_m is the reinforcement ratio in the meridional direction, ρ_{ph} is the prestressing tendon ratio in the hoop direction, ρ_{pm} is the prestressing tendon ratio in the meridional direction, σ_h is the hoop-direction normal stress due to dead load, internal pressure, prestress, and seismic load, σ_m is the meridional-direction normal stress due to dead load, internal pressure, prestress, and seismic load, f_y is the

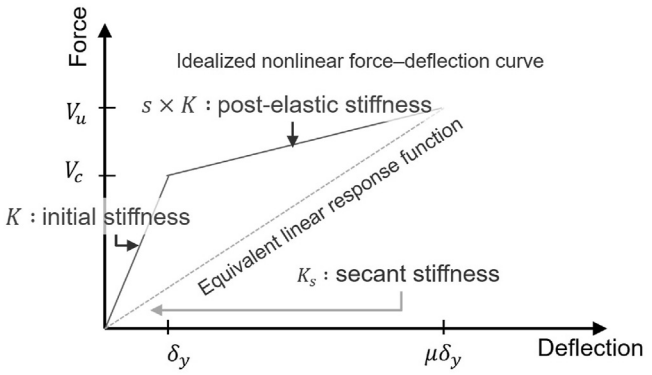

Fig. 5. Force-deflection curve and related parameters for calculating F_μ [8,47].

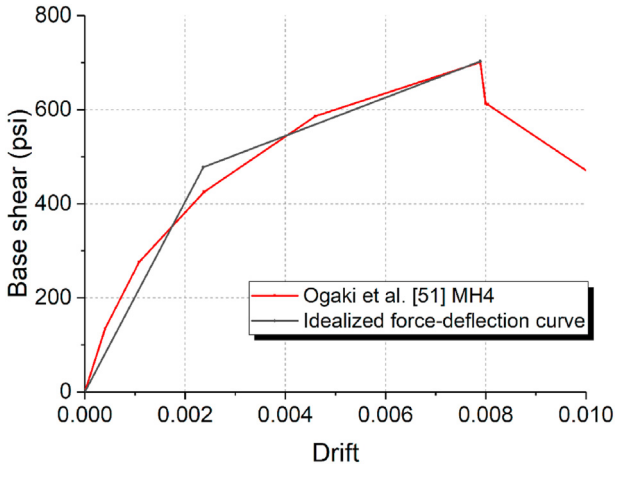

Fig. 6. Idealized force deflection curve considering the envelope of MH 4 of Ogaki et al. [51].

yield stress of reinforcement, and f_{py} is the yield stress of the pre-stressing tendon.

4.2. Elastic scale factor

The elastic scale factor is a constant that is used to estimate the level of ground motion that causes the structure to reach its elastic limit state. The elastic scale factor F_{SE} can be estimated by Ref. [8]:

$$F_{SE} = \frac{C_s - D_{ns}}{D_s + \Delta C_s} \tag{5}$$

where C_s is the capacity of the target structure, D_{ns} is the demand imposed on the structure by a non-seismic load, D_s is the demand imposed on the structure by a seismic load, and ΔC_s is the change in the capacity of the structure due to the seismic load. All the variables in (5) should be taken as stress-terms in the following manner: the shear stress (C_s) is calculated as the base shear capacity divided by effective cross-sectional area of the containment wall considering equations (1)–(4), the seismic demand (D_s) is taken as the shear stress at the base induced by seismic loading, the non-seismic demand (D_{ns}) is the stress induced by other non-seismic loads such as gravity and pressure, and the effects of vertical ground motion on shear strength are categorized as the change in capacity (ΔC_s). The elastic scale factor should be taken as the minimum value calculated in the overall analysis that satisfies the safety condition during the entire ground motion duration.

4.3. Inelastic energy absorption factor

The inelastic energy absorption factor is used for computing the effects of the inelastic behavior of a structure. These include changes in the dynamic frequency and pinching of the hysteresis curve in the inelastic range. It is possible to estimate the median capacity of a structure after calculating both the elastic scale factor and energy absorption factor. In this study, the effective frequency/effective damping method is adopted to calculate the inelastic energy absorption factor as follows:

$$F_\mu = \left(\frac{f_e/f}{f_s/f}\right)^2 \frac{S_A(f,\beta)}{S_A(f_e,\beta_e)} \tag{6}$$

where F_μ is the inelastic energy absorption factor, f is the natural frequency (first-mode) of the structure, f_s is the secant frequency, f_e is the effective frequency, S_A is the spectral acceleration obtained from the ground input to the structure, β_e is the effective damping value, and β is the median damping value.

Referring to Kennedy et al. [54], the effective frequency/effective damping method replaces the nonlinear response curve with an equivalent linear response function with lower stiffness and increased damping as shown in Fig. 5. Therefore, the secant frequency and the effective frequency can be calculated using the following equation:

$$\frac{f_s}{f} = \sqrt{\frac{K_s}{K}} = \sqrt{\frac{1+s(\mu-1)}{\mu}},\ \mu = \frac{\sum w_i \breve{\delta}_{Ti}}{\sum w_i \breve{\delta}_{ei}} \tag{7}$$

where K is the initial stiffness of the structure, K_s is the secant stiffness of the structure, s is the ratio between the initial stiffness and the post-elastic stiffness, and μ is the ductility of the structure, w_i is the weight of each story, $\breve{\delta}_{Ti}$ is the median maximum deflection of each story, and $\breve{\delta}_{ei}$ is the median elastic deflection of each story scaled to the level at which the critical story yields. The secant stiffness represents the minimum effective stiffness K_s during the nonlinear response. A previous study also suggested that the method should take into account the nonlinear response averaged for overall displacement [54]:

$$\frac{f_e}{f} = (1-A) + A\left(\frac{f_s}{f}\right),\ A = C_F\left(1 - \frac{f_s}{f}\right) \le 0.85 \tag{8}$$

$$\beta_e = \left(\frac{f_e/f}{f_s/f}\right)^2 (\beta + \beta_h),\ \beta_h = 0.11\left(1 - \frac{f_s}{f}\right) \tag{9}$$

where A and C_F are empirically determined coefficients and β_h is the pinched hysteretic damping value.

The stiffness ratio, s, and ductility, μ, are required to estimate the inelastic absorption factor and therefore the experimental results of a previous structural study were used to develop the idealized force–deflection curve of the containment structure (Fig. 6) [51]. The ductility estimated from Fig. 6 is about 3.343, which is similar with the value suggested by Lee and Song [34]. As described earlier, the median seismic capacity of the structure can be calculated using the elastic scale factor and the inelastic energy absorption factor as follows:

$$A_m = A_{REF}\breve{F}_{SE}\breve{F}_\mu = A_{REF}\breve{F}_S \tag{10}$$

where A_m is the median seismic capacity of the structure, which is expressed as the corresponding ground motion parameter (e.g., PGA, spectral acceleration), A_{REF} is the ground motion parameter of reference earthquakes used for seismic fragility analysis, $\breve{F}_{SE}$ is the median elastic scale factor, $\breve{F}_\mu$ is the median inelastic energy absorption factor, and $\breve{F}_S$ is the median scale factor expressed as the product of $\breve{F}_{SE}$ and $\breve{F}_\mu$.

The median capacity can be calculated when all the basic variables are set to median value. Thus, it is possible to investigate the effects of uncertainty in variables calculated based on median capacity, by setting certain basic variables to values that are far from the median value, considering the uncertainty and randomness involved in the basic variables. This is the main idea for the calculation procedure for effects of uncertainty in the fragility curve and will be discussed in later sections.

Table 5
Logarithmic standard deviations of considered variables in fragility analysis [8,11,12].

Considered variables in fragility analysis	Logarithmic standard deviation	
	β_{Ri}	β_{Ui}
Spectral shape	0.14	0
Horizontal peak response	0.1	0
Vertical peak response	0.34	0
Structural damping ratio[a]	0	Median damping ratio: 0.07 Damping ratio with 1σ : 0.05
Modeling-frequency	0	0.17
Modeling-mod eshape	0	0.06
Mode combination	0.05	0
Time history simulation	0	0.05
Foundation structure interaction	0	0.05
Concrete strength	0	0.15
Reinforcement yield strength	0	0.11
Inelastic energy absorption factor	[b]	[b]

[a] The logarithmic standard deviation for damping should be calculated from several analyses considering its median damping value and the damping value at 1σ of the standard deviation.
[b] The logarithmic standard deviation for inelastic energy absorption factor is calculated by using equation (16).

4.4. Effects of uncertainty and randomness

The methodology of the EPRI guideline suggested that the

Table 6
Calculation results for the median elastic scale factor, F_{SE}.

Ground motion No.	Shear force (kips)	Bending moment (kips-ft)	Axial force (kips)	F_{SE}
1	2.334×10^4	3.762×10^6	2.136×10^2	8.177
2	2.304×10^4	3.398×10^6	10.05×10^3	8.197
3	2.317×10^4	3.237×10^6	14.13×10^3	8.148
4	2.612×10^4	3.366×10^6	15.63×10^3	7.381
5	2.389×10^4	3.602×10^6	9.921×10^3	7.871
6	2.336×10^4	3.528×10^6	14.19×10^3	7.919
7	2.479×10^4	3.792×10^6	4.898×10^3	7.694
8	2.487×10^4	3.875×10^6	9.240×10^3	7.518
9	2.410×10^4	3.646×10^6	4.174×10^3	7.955
10	2.298×10^4	3.654×10^6	4.246×10^3	8.216
11	2.456×10^4	3.897×10^6	8.636×10^3	7.586
12	2.698×10^4	3.542×10^6	9.516×10^3	7.264
13	2.015×10^4	3.362×10^6	1.092×10^3	9.340
14	2.361×10^4	3.540×10^6	2.566×10^3	8.184
15	2.343×10^4	3.000×10^6	8.224×10^3	8.419
16	2.528×10^4	4.017×10^6	2.504×10^3	7.523
17	2.274×10^4	3.495×10^6	6.063×10^3	8.326
18	3.178×10^4	3.818×10^6	7.625×10^3	6.364
19	2.745×10^4	3.320×10^6	7.509×10^3	7.333
20	2.419×10^4	3.658×10^6	4.887×10^3	7.909
21	2.250×10^4	3.774×10^6	0.360×10^2	8.388
22	2.287×10^4	3.469×10^6	2.295×10^3	8.428
23	2.300×10^4	3.642×10^6	3.750×10^3	8.232
24	2.206×10^4	3.683×10^6	1.734×10^3	8.509
25	2.509×10^4	3.948×10^6	4.239×10^3	7.558
26	2.031×10^4	3.501×10^6	0.413×10^2	9.212
27	2.243×10^4	3.428×10^6	4.953×10^3	8.489
28	1.727×10^4	2.605×10^6	13.42×10^3	10.57
29	2.332×10^4	2.663×10^6	14.16×10^3	8.492
30	2.509×10^4	3.177×10^6	10.84×10^3	7.827
Median	2.340×10^4	3.541×10^6	5.508×10^3	8.163
COV	0.1049	0.0951	0.6968	0.0922

failure probabilities of structure at varying PGA levels could be estimated by using logarithmic standard deviation, which evaluating the effects of uncertainty of basic variables on the seismic demand and seismic capacity of the structures [8]. The seismic fragility curves developed in this study are based on the approximate second moment procedure suggested by the EPRI guideline; therefore, it is necessary to calculate the logarithmic standard deviations that takes into account the randomness and uncertainty in basic variables such as the spectral shape of the ground motion, material properties of concrete, damping of the structure, modeling of the target structures, and so on [8]. In the approximate second moment procedure, the effects of randomness and uncertainty in certain variables are reflected as a logarithmic standard deviation which can be calculated by:

$$\beta_i = \frac{1}{|\phi|} \ln\left(\frac{F_{S\phi\sigma_i}}{\breve{F}_S}\right) \tag{11}$$

where β_i is the logarithmic standard deviation which accounts for the uncertainty or randomness in the i-th basic variable, $\breve{F}_S$ is the median scale factor, $F_{S\phi\sigma_i}$ is the scale factor that is calculated when the i-th basic variable is set at the standard deviation level of $\phi\sigma_i$, and ϕ is the z value of the i-th basic variable at this setting.

The ϕ value is typically 1 when the basic variable set at the standard deviation level of $\phi\sigma_i$ decreases the resulting scale factor. In this study, the $F_{S\phi\sigma_i}$ values were calculated by referring to the EPRI guideline or the material property data reported in previous studies (Table 1) [8,9]. The guideline suggests that the β_i value for

Table 7
Calculation results for the median inelastic energy absorption factor, F_{μ}.

Ground motion No.	f_e/f_s	$S_A(f,\beta)$ (g)	$S_A(f_e,\beta_e)$ (g)	F_{μ}
1	1.232	0.4806	0.3448	1.732
2	1.232	0.4783	0.3625	1.640
3	1.232	0.4278	0.3030	1.755
4	1.232	0.4181	0.3317	1.567
5	1.232	0.4476	0.3584	1.552
6	1.232	0.4347	0.3146	1.717
7	1.232	0.4508	0.3161	1.772
8	1.232	0.4856	0.2987	2.020
9	1.232	0.4332	0.2997	1.797
10	1.232	0.4610	0.3165	1.810
11	1.232	0.4698	0.3051	1.913
12	1.232	0.4552	0.2879	1.965
13	1.232	0.4268	0.3277	1.619
14	1.232	0.4563	0.3381	1.677
15	1.232	0.4482	0.3286	1.695
16	1.232	0.4866	0.3566	1.696
17	1.232	0.4472	0.3795	1.464
18	1.232	0.4738	0.3266	1.803
19	1.232	0.4347	0.3458	1.562
20	1.232	0.4639	0.3347	1.722
21	1.232	0.4622	0.3141	1.828
22	1.232	0.4672	0.3275	1.773
23	1.232	0.4510	0.2973	1.886
24	1.232	0.4850	0.3367	1.790
25	1.232	0.4805	0.2931	2.037
26	1.232	0.4284	0.3286	1.620
27	1.232	0.4794	0.3346	1.781
28	1.232	0.4149	0.2919	1.766
29	1.232	0.4541	0.3408	1.656
30	1.232	0.4684	0.3158	1.843
Median	1.232	0.4558	0.3276	1.761
COV	0	0.0465	0.0701	0.0775

each basic variable is based on their effects on the seismic capacity of the structure and can be expressed in the following manner [8,9]:

$$A_{\phi\sigma_i} = A_m e^{\phi\beta_{i,g}} \tag{12}$$

where $A_{\phi\sigma_i}$ is the capacity when the i-th basic variable is set at the standard deviation level of $\phi\sigma_i$, $\check{D}$ is the median demand value, and $\beta_{i,g}$ is the logarithmic standard deviation value suggested in EPRI TR-103959.

Equation (12) described the direct relation between the A_m and $A_{\phi\sigma_i}$. Therefore, the user could use the $\beta_{i,g}$ values described in Table 5 directly as β_i values using (11). Moreover, it is possible to calculate the β_i values from β_{ig} by following the method suggested in the appendix of the EPRI guideline:

$$D_{s,\,\phi\sigma_i} = \check{D}_s e^{\beta_{i,g}} \tag{13}$$

$$C_{s,\,\phi\sigma_i} = \check{C}_s e^{-\beta_{i,g}} \tag{14}$$

$$\Delta C_{s,\,\phi\sigma_i} = \Delta\check{C}_s e^{-\beta_{i,g}} \tag{15}$$

where $D_{s,\,\phi\sigma_i}$ is the seismic demand with the standard deviation $\phi\sigma_i$, $\check{D}_s$ is the median seismic demand, $C_{s,\,\phi\sigma_i}$ is the seismic capacity with the standard deviation $\phi\sigma_i$, $\check{C}_s$ is the median seismic capacity, $\Delta C_{s,\,\phi\sigma_i}$ is the change in seismic capacity with the standard deviation $\phi\sigma_i$, and $\Delta\check{C}_s$ is the median change in seismic capacity.

Unlike the other basic variables, the β_i values of the structural damping ratio can be estimated after calculating the scale factor $F_{S\phi\sigma_i}$ separately. For this reason, the analysis is done twice to gather the response of the structure with different damping ratios. In addition, the β_i values due to the variability in inelastic energy absorption factor should be evaluated by equation (16) referring the suggestions of EPRI TR-103959 guideline [8].

$$\beta_{R\_\check{F}_\mu} = 0.4\left[0.06 + 0.03\left(\check{F}_\mu - 1\right)\right]$$
$$\beta_{U\_\check{F}_\mu} = C_U\left(\check{F}_\mu - 1\right) \tag{16}$$

where $\beta_{R\_\check{F}_\mu}$ is the logarithmic standard deviation that takes account of the randomness in inelastic energy absorption factor, $\beta_{R\_\check{F}_\mu}$ is the logarithmic standard deviation that takes account of the uncertainty in inelastic energy absorption factor, $\check{F}_\mu$ is the median inelastic energy absorption factor, and C_U is the empirical constant.

As discussed above, the value of ϕ is typically 1 when $\phi\sigma_i$ decreases the resulting scale factor. In this case, (14) and (15) should be modified to decrease $C_{s,\,\phi\sigma_i}$ and $\Delta C_{s,\,\phi\sigma_i}$ using $-\beta_{i,g}$. Thereafter, the β_i values can be calculated by updating the $F_{S_{\phi\sigma_i}}$ values with the parameters resulting from equations (13)–(15). The logarithmic standard deviation β_i values are then calculated for both uncertainty (β_{Ui}) and randomness (β_{Ri}) using (11). Consequently, the β_i value of each basic variable is used to calculate the β values for total randomness and uncertainty:

$$\beta_R = \sqrt{\sum_i {\beta_{Ri}}^2},\ \beta_U = \sqrt{\sum_i {\beta_{Ui}}^2} \tag{17}$$

where β_R is the logarithmic standard deviation that takes account of the randomness of the overall basic variables, β_{Ri} is the β_i value for the randomness in the i-th basic variable, β_U is the logarithmic standard deviation that takes accounts of the uncertainty of the overall basic variables, and β_{Ui} is the β_i value for the uncertainty in the i-th basic variable.

Finally, the equation for the fragility curve can be expressed using the double log normal model as follows [8,11,12]:

$$P_f(a) = \Phi\left(\frac{\ln(a/A_m) + \beta_U\Phi^{-1}(Q)}{\beta_R}\right) \tag{18}$$

where $P_f(a)$ is the probability of failure of the structure, Φ is the logarithmic distribution function, a is the PGA (g), and Q is the non-exceedance probability of each fragility curve, typically suggested as 5 %, 50 %, and 95 % to present the change in the fragility curve when considering the effects of uncertainty (β_U) in fragility curve.

Table 8
Fragility analysis parameters based on spectral-matched time histories.

Ground motion No.	F_{SE}	F_μ	A_m (g)	β_R	β_U	HCLPF (g)
1	8.177	1.732	2.833	0.1888	0.3039	1.257
2	8.197	1.640	2.688	0.1875	0.2907	1.221
3	8.148	1.755	2.859	0.1876	0.2944	1.291
4	7.381	1.567	2.313	0.1871	0.2931	1.047
5	7.871	1.552	2.443	0.1873	0.2803	1.130
6	7.919	1.717	2.720	0.1874	0.2848	1.248
7	7.694	1.772	2.727	0.1883	0.3017	1.215
8	7.518	2.020	3.038	0.1884	0.3189	1.315
9	7.955	1.797	2.858	0.1884	0.2940	1.290
10	8.216	1.810	2.974	0.1884	0.3038	1.320
11	7.586	1.913	2.903	0.1882	0.3050	1.286
12	7.264	1.965	2.854	0.1883	0.3167	1.241
13	9.340	1.619	3.023	0.1884	0.2843	1.386
14	8.184	1.677	2.745	0.1883	0.2932	1.240
15	8.419	1.695	2.854	0.1877	0.2940	1.289
16	7.523	1.696	2.551	0.1884	0.3250	1.094
17	8.326	1.464	2.438	0.1874	0.2926	1.105
18	6.364	1.803	2.295	0.1882	0.3014	1.023
19	7.333	1.562	2.291	0.1876	0.2794	1.060
20	7.909	1.722	2.725	0.1881	0.2910	1.236
21	8.388	1.828	3.067	0.1891	0.3060	1.355
22	8.428	1.773	2.988	0.1886	0.3011	1.332
23	8.232	1.886	3.105	0.1886	0.3043	1.377
24	8.509	1.790	3.046	0.1887	0.3079	1.342
25	7.558	2.037	3.080	0.1889	0.3050	1.363
26	9.212	1.620	2.985	0.1886	0.2909	1.353
27	8.489	1.781	3.023	0.1882	0.3108	1.327
28	10.57	1.766	3.734	0.1875	0.3190	1.619
29	8.492	1.656	2.812	0.1873	0.2877	1.284
30	7.827	1.843	2.885	0.1879	0.2992	1.291
Median	8.163	1.761	2.856	0.1883	0.3002	1.288
COV	0.0922	0.0775	0.1047	0.0029	0.0386	0.0962

5. Results and discussions

5.1. Time history response

The structural analysis was performed 60 times considering the uncertainty in structural damping discussed in Section 4. The earthquake time histories produced by the spectral matching were integrated in terms of the displacement histories and assigned to the basemat of the lumped mass model as boundary conditions. The ground motions in two horizontal directions and one vertical direction are imposed simultaneously. A time history with the same shape but a reduced magnitude equal to 0.65 times that of the horizontal ground motion is imposed referring NUREG CR-0098 [55].

To assess F_{SE} properly, the structural analysis results in Table 6 were collected considering the following. The guideline suggests combining 100% of the response in one governing direction with 40 % of the responses from the other two directions to calculate the

Table 9
Ground motion parameters used in correlation analysis.

Ground motion parameter	Definition	Reference
Peak ground acceleration (g)	$PGA = \max\left\|\ddot{u}_g(t)\right\|$	
Peak ground velocity (m/s)	$PGV = \max\left\|\dot{u}_g(t)\right\|$	
Peak ground displacement (m)	$PGD = \max\left\|u_g(t)\right\|$	
PGV/PGA (s)	PGV/PGA	Kramer [56]
$(S_a)_n$(g)	Spectral acceleration (5% damping) at the 1st natural frequency of the structure	
Significant duration $D_{S_{5-95\%}}$ (s)	$D_{s_{xy}} = t_y - t_x,\ x = \frac{\int_0^{t_x}(\ddot{u}_g(t))^2 dt}{\int_0^{t_{total}}(\ddot{u}_g(t))^2 dt}$	Bommer et al. [57]
Arias intensity	$I_a = \frac{\pi}{2g}\int_0^{t_{total}}(\ddot{u}_g(t))^2 dt$	Arias [58]
Acceleration RMS (g)	$A_{rms} = \sqrt{\frac{1}{t_{total}}\int_0^{t_{total}}(\ddot{u}_g(t))^2 dt}$	Housner [59]
Velocity RMS (m/s)	$V_{rms} = \sqrt{\frac{1}{t_{total}}\int_0^{t_{total}}(\dot{u}_g(t))^2 dt}$	Kramer [56]
Displacement RMS (m)	$D_{rms} = \sqrt{\frac{1}{t_{total}}\int_0^{t_{total}}(u_g(t))^2 dt}$	Kramer [56]
Characteristic intensity	$I_c = (A_{rms})^{\frac{2}{3}}\sqrt{t_{total}}$	Park et al. [60]
Specific energy density (m^2/s)	$SED = \int_0^{t_{total}}(\dot{u}_g(t))^2 dt$	
Cumulative absolute velocity (m/s)	$CAV = \int_0^{t_{total}}(\ddot{u}_g(t))^2 dt$	Reed and Kassawara [61]
Acc. spectrum intensity (g· s)	$ASI = \int_{0.1}^{0.5} S_{a,\,5\%}(T)dT$	Housner [62]
Vel. spectrum intensity (m)	$VSI = \int_{0.1}^{2.5} S_{v,\,5\%}(T)dT$	Housner [62]
Housner intensity (m)	$HI = \int_{0.1}^{2.5} PSV(T,\,5\%)dT$	Housner [62]
Sustained maximum acceleration (g)	SMA = the 3rd highest PGA	Nuttli [63]
Sustained maximum velocity (cm/s)	SMV = the 3rd highest PGV	Nuttli [63]
Effective design acceleration (g)	$A_D = 1.25A_{3F}$ A_{3F}: 3rd highest PGA from the filtered time history	Reed and Kassawara [61]
A 95 parameter (g)	$A_{95} = 0.764{I_a}^{0.438}$	Sarma and Yang [64]
Predominant period (s)	T_p	Kramer [56]

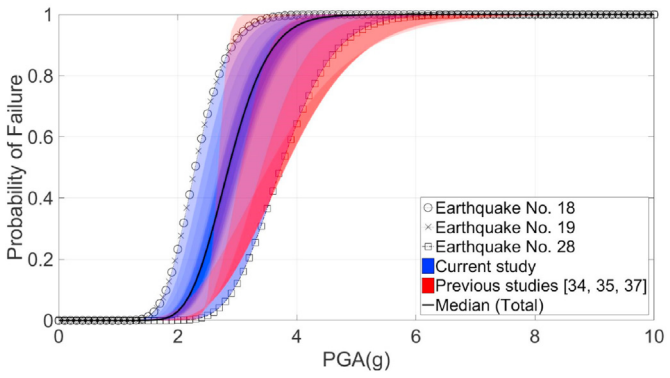

Fig. 7. Comparison between fragility curves resulting from different time histories.

median response [8,11,12]. The maximum tangential shear stress from one horizontal response is not affected by the other horizontal response, while the axial force from vertical response contributes to the maximum tangential shear stress from both horizontal directions [48]. Therefore, the five demands, i.e., horizontal shear forces in two directions, bending moments from two horizontal directions, and the axial force in the vertical direction were collected for the entire earthquake duration. Then, the elastic scale factor corresponding to each horizontal response was calculated using (5). Finally, a set of three demands that results in the smallest elastic scale factor was taken to calculate F_{SE}.

The COVs of the shear force and bending moment are below 0.15. The trend of the vertical responses shows that the median value was highly affected by the time histories used in the analysis and have a high COV value of 0.6968. Nonetheless, the vertical response is a non-dominant component and has no significant effect on F_{SE}. Consequently, the median value and COV of F_{SE} are 8.163 and 0.0922 when considering all the data, respectively.

5.2. Seismic fragility analysis

The information required to calculate the median value of F_μ as well as the resulting F_μ is summarized in Table 7. As specified by equations (6)–(9), the calculation of the inelastic energy absorption factor requires the spectral acceleration value corresponding to the initial damping and the frequency, as well the acceleration value corresponding to the effective damping and effective frequency. The ratio between the effective frequency and the secant frequency (f_e/f_s) was assumed to be identical in all cases, and the spectral

accelerations required for the analysis were computed using SeismoMatch software. The resulting median value of the inelastic energy absorption factor is 1.761, and COV is just about 0.077. The inelastic energy absorption factors based on earthquake no. 8 and no. 25 have higher value compared to the other data. However, it is shown that both time histories have differences in their earthquake characteristic such as significant duration, Arias intensity, Acceleration RMS, characteristic intensity, and SMA.

The fragility curves developed using the method described in Section 4 are shown in Fig. 7. The values of the several fragility parameters are summarized in Table 8. Sets of median capacity A_m, beta values for randomness, β_R, and beta values for uncertainty β_U were calculated using equations (10)–(16). In previous studies [34,35,37], the high confidence of low probability of failure (HCLPF) and the median capacity of the containment structure in OPR-1000 were calculated to be 1.20 g–1.41 g and 2.681 g–3.81 g, respectively, based on the shear failure criteria. The fragility curves developed in previous studies are depicted using the red-shaded area in Fig. 7.

In overall, the median capacity and HCLPF values in this study are slightly lower than those reported in the previous studies. The median values of the A_m, HCLPF, β_R, and β_U calculated from all 30 analysis results are 2.856, 1.288, 0.1883, and 0.3002, respectively. The COVs of the A_m, HCLPF, β_R, and β_U are 0.1047, 0.0962, 0.0029, and 0.0386, respectively. The fragility curves result from earthquake No. 18, No. 19, and No. 28 tend to have higher variance

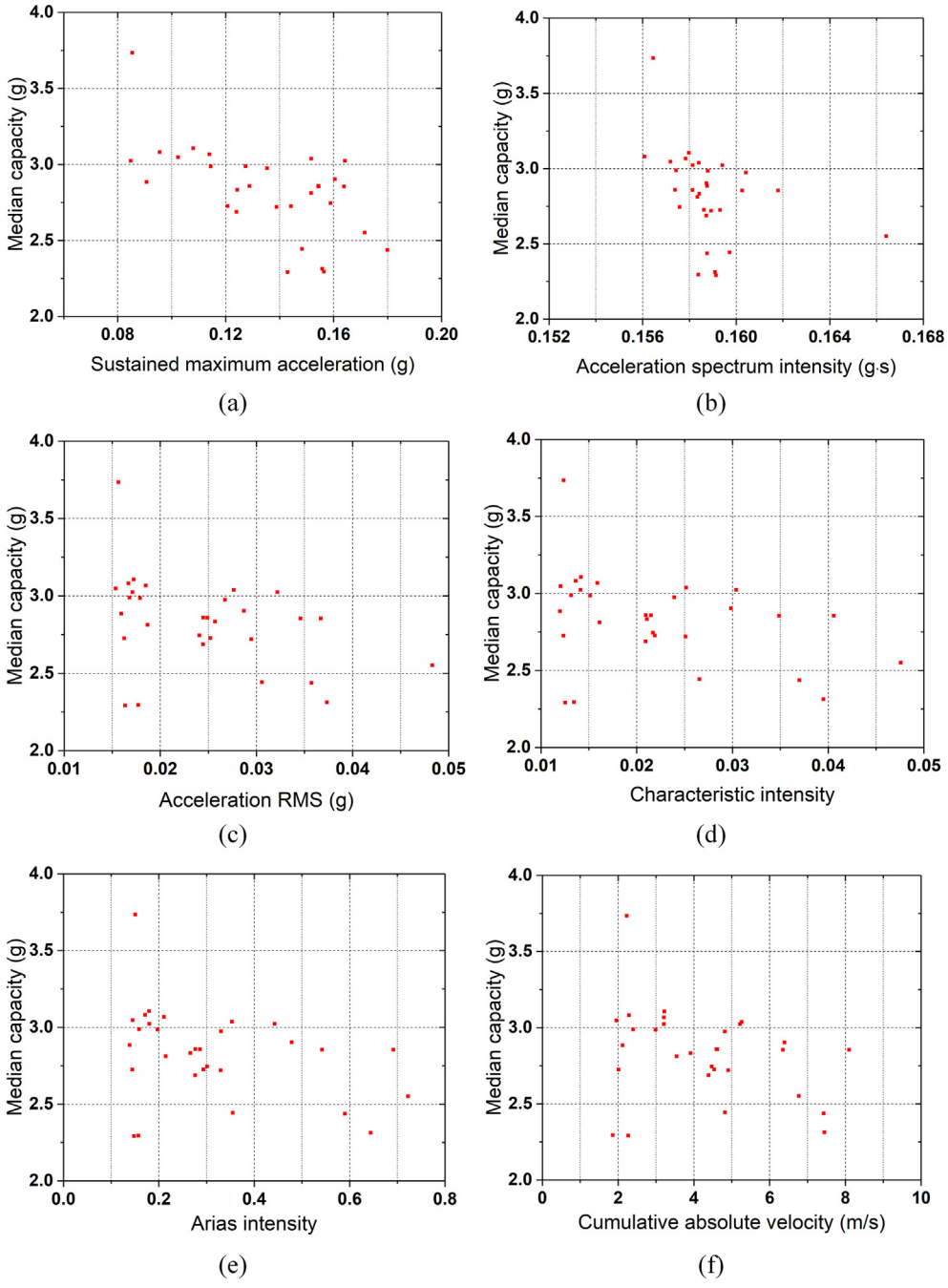

Fig. 8. Relationship between median capacity and ground motion parameters.

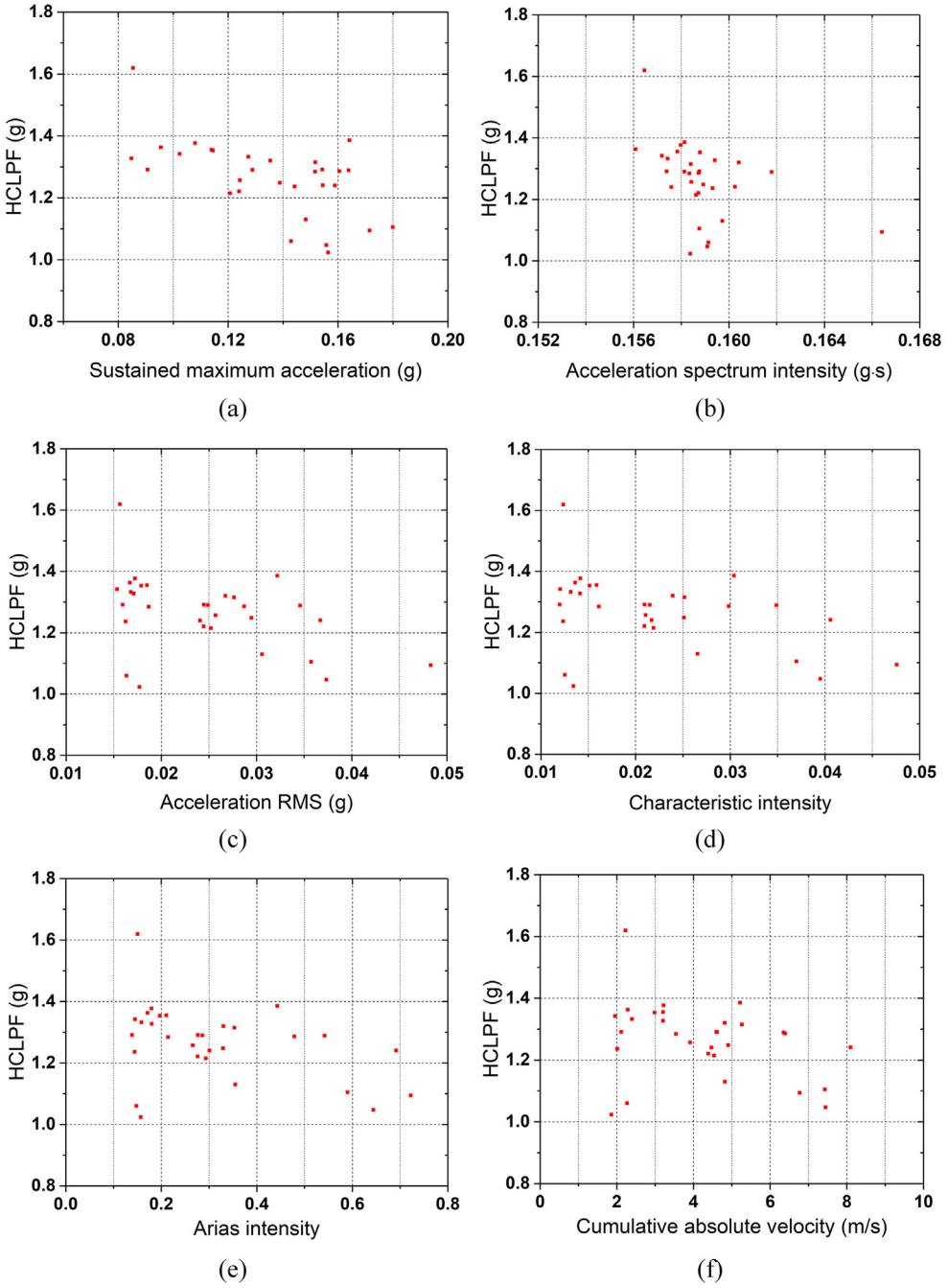

Fig. 9. Relationship between HCLPF and ground motion parameters.

compared to the others, as it shown in Fig. 7. These time histories have similarity in their level of acceleration RMS, level of characteristic intensity, and significant duration shorter than others, while have large difference in their sustained maximum acceleration. Consequently, it is observed that the HCLPF estimated in this study are similar with the values reported in previous studies [34,35,37]. Furthermore, the differences in the fragility parameters exist between several analysis cases, and the sustained maximum acceleration seems to correlated with these differences.

5.3. Correlation between fragility parameters and earthquake characteristics

In this section, possible correlations between the fragility parameters and earthquake characteristics are investigated. In totally, 21 ground motion parameters suggested by previous studies [56–64] are selected for the correlation analysis. The information for selected ground motion parameters is described in Table 9.

5.3.1. Median capacity vs. ground motion parameters

The correlation analyses for median capacity are described in Fig. 8. The earthquake characteristic showing the strongest correlation with the median capacity is SMA with the R^2 of 0.3666. The other parameters showing high R^2 value are acceleration spectrum intensity (ASI), followed by acceleration RMS, characteristic intensity, Arias intensity, and cumulative absolute velocity (CAV). The higher values of SMA, ASI, acceleration RMS, characteristic

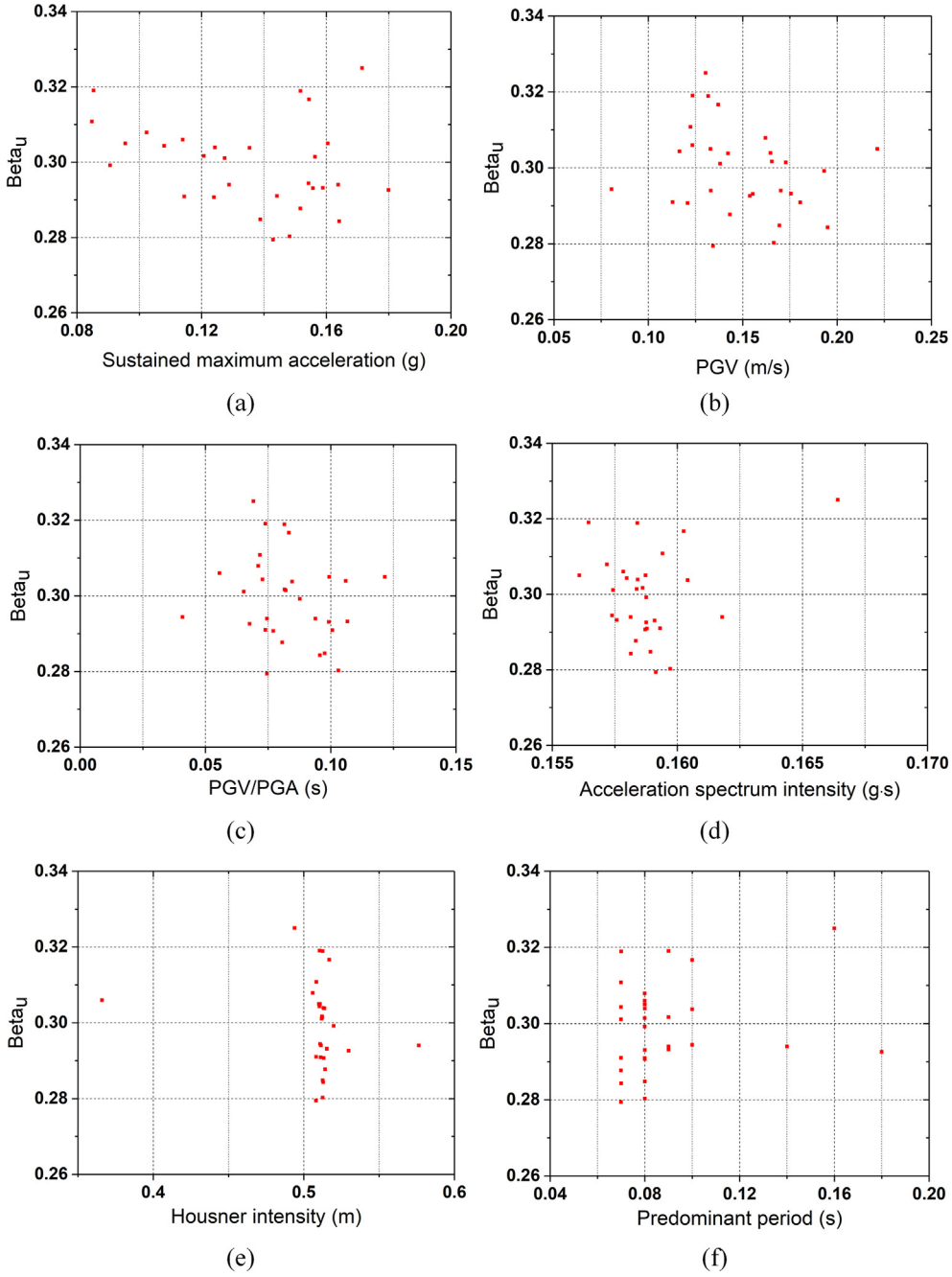

Fig. 10. Relationship between β_U and ground motion parameters.

intensity, Arias intensity, and CAV tend to result in lower median capacity. In contrast with expectations, the relationship between significant duration and the fragility parameters is considered to be weak, since the R^2 value between median capacity and significant duration is only about 0.055. The differences in range of parameters such as acceleration RMS, characteristic intensity, Arias intensity and CAV seems not to have significant correlation with the median capacity. The SMA and ASI parameters show high R^2 values for median capacity, and all the time histories share a similar range. For this reason, SMA and ASI are regarded as the ground motion parameters most strongly related with the median capacity estimated from the methodology in this study.

5.3.2. HCLPF vs. ground motion parameters

The correlation analyses for HCLPF are shown in Fig. 9. The correlation analyses for HCLPF shows a trend similar to that observed in median capacity. The parameters showing high R^2 value with HCLPF are SMA, followed by ASI, acceleration RMS, characteristic intensity, Arias intensity, and CAV. The R^2 value between HCLPF and SMA is about 0.3545. The differences in range of parameters such as acceleration RMS, characteristic intensity, Arias intensity and CAV are also similar to the observation in median capacity. In the same manner, SMA and ASI are deemed to be the ground motion parameters most strongly related with the HCLPF.

5.3.3. β_U vs. ground motion parameters

The correlation analyses for β_U are described in Fig. 10. The correlation analyses for β_U shows a different trend to median capacity and HCLPF. First of all, the R^2 value between ground motion parameters and β_U are lower than the R^2 values for median capacity and HCLPF. The sustained maximum acceleration demonstrates the highest R^2 value with β_U at only 0.0683. PGV is the ground motion parameter showing the second highest R^2 at 0.0514, followed by the PGV/PGA, ASI, Housner intensity and predominant period. In addition to these low R^2 values, the trend between β_U and the ground motion parameters is difficult to observe. For example, in Fig. 10 (d), data resulting from earthquake No. 16 seems to be a statistical outlier, since it is distinct from the region occupied by other data. Nonetheless, this value of β_U has a slight difference of 9.5 % to the median value. As aforementioned above, the COVs of β_R and β_U are much lower than COVs of median capacity and HCLPF. In other words, randomness and uncertainty of the fragility curves do not appear to significantly vary with ground motion parameters, compared to the median capacity and HCLPF (see Fig. 10).

Consequently, it can be noted that using the ground motion data of the Gyeongju earthquake for seismic fragility analysis provides similar results to the other data. Based on the analysis results including all the data, the COVs of the fragility parameters are within 0.11. The time histories from the Gyeongju earthquake shows significant differences with the other time histories in terms of significant duration, Arias intensity, and characteristic intensity. However, the correlation analysis suggested that the differences in these characteristics are barely affected by the fragility parameter. Instead, sustained maximum acceleration seems to more significantly related with the calculated median capacity and HCLPF of the containment structure.

6. Conclusions

In this study, the effects of ground motion parameters on the seismic fragility of the OPR-1000 reactor containment were investigated. Seismic fragility analyses were undertaken based on 30 recorded ground motions around the world, including those of the Gyeongju earthquake. The fragility parameters resulting from each earthquake time history were compared with those resulting from others. Furthermore, correlation analyses between the fragility parameters and ground motion characteristics were performed to investigate ground motion parameters that strongly affect the seismic capacity of the structure. The findings and conclusions of this study are summarized in the following.

- The earthquake characteristics such as significant duration, Arias intensity, characteristic intensity generally showed larger COVs, and these characteristics shown relatively smaller values in Gyeongju ground motions. In contrast, the sustained maximum acceleration showed smaller COV in the time histories, compared to the other earthquake characteristics that are previously noted.
- The median capacity and HCLPF in terms of PGA were estimated to be 2.856 g and 1.288 g, respectively, when considering all the ground motions. The COVs of median capacity and HCLPF were 0.1047 and 0.0962, respectively. In overall, the differences between β_R and β_U resulting from each time history are unclear.
- Correlation analyses revealed that, except for sustained maximum acceleration, most of the earthquake characteristics are weakly correlated with the fragility parameters. The sustained maximum acceleration showed a relatively high correlation with the median capacity and HCLPF than other ground motion parameters.
- Future study is on the way to demonstrate the correlation between the sustained maximum acceleration and the capacity of the containment structure. Careful consideration of the sustained maximum acceleration could be helpful in developing highly reliable seismic fragility curves with a lower uncertainty using a reasonable number of ground motions.

Declaration of competing interest

The authors declare that they have no known competing financial interests or personal relationships that could have appeared to influence the work reported in this paper.

Acknowledgment

This work was supported by the Korea Institute of Energy Technology Evaluation and Planning (KETEP) grant funded by the Korea government (MOTIE) (No. 20201510100020, Research on analysis of earthquake & fault characteristics and seismic performance improvement to respond against earthquake hazards).

References

[1] ASCE, Seismic Design Criteria for Structures, Systems, and Components in Nuclear Facilities, American Society of Civil Engineers, Reston, VA, 2005.
[2] ACI Committee 349, Code Requirements for Nuclear Safety-Related Concrete Structures (ACI 349-13) and Commentary, American Concrete Institute, Farmington Hills, 2013.
[3] ASCE, Seismic Analysis of Safety-Related Nuclear Structures and Commentary, American Society of Civil Engineers, 2014.
[4] U.S. AEC, Design Response Spectra for Seismic Design of Nuclear Power Plants Revision 1, Regulatory Guide 1.60, U.S. Atomic Energy Commission, Washington, 1973.
[5] R.P. Kennedy, C.A. Cornell, R.D. Campbell, S. Kaplan, H.F. Perla, Probabilistic seismic safety study of an existing nuclear power plant, Nucl. Eng. Des. 59 (2) (1980) 315–338.
[6] D.A. Wesley, P.S. Hashimoto, Seismic Structural Fragility Investigation for the Zion Nuclear Power Plant. Seismic Safety Margins Research Program (Phase 1), 1981. Lawrence Livermore National Laboratory.
[7] U.S. NRC, A guide to the performance of probabilistic risk assessments for nuclear power plants, 1983. U.S. Nuclear Regulatory Commission, Washington DC NUREG/CR-2300.
[8] J.W. Reed, R.P. Kennedy, Methodology for Developing Seismic Fragilities, 1994. Final Report TR-103959, EPRI.
[9] U.S. NEI, Methodology for Performing Aircraft Impact Assessments for New Plant Designs, 2011. NEI 07-13 Revision 8P.
[10] Working Group on Quantification of Uncertainties, Uncertainty and Conservatism in the Seismic Analysis of Nuclear Facilities, American Society of Civil Engineers, New York, USA, 1986.
[11] EPRI, Seismic Fragility Application Guide. EPRI 1002988, Electric Power Research Institute (EPRI), Palo Alto, CA, USA, 2002.
[12] EPRI, Seismic Fragility Application Update Guide, Electric Power Research Institute (EPRI), Palo Alto, CA, USA, 2009. EPRI 1019200.
[13] EPRI, Seismic Evaluation Guidance: Screening, Prioritization and Implementation Details (SPID) for the Resolution of Fukushima Near-Term Task Force Recommendation 2, vol. 1, 2012. Seismic (No. 1025287).
[14] EPRI, High Frequency Program: Application Guidance for Functional Confirmation and Fragility Evaluation, Electric Power Research Institute (EPRI), Palo Alto, CA, USA, 2015. EPRI 3002004396.
[15] C.S. Kumar, V. Hassija, K. Velusamy, V. Balasubramaniyan, Integrated risk assessment for multi-unit NPP sites—a comparison, Nucl. Eng. Des. 293 (2015) 53–62.
[16] T. Zhou, M. Modarres, E.L. Droguett, An improved multi-unit nuclear plant seismic probabilistic risk assessment approach, Reliab. Eng. Syst. Saf. 171 (2018) 34–47.
[17] S.H. Eem, I.K. Choi, B.J. Yang, S.Y. Kwang, Methodology of seismic-response-correlation-coefficient calculation for seismic probabilistic safety assessment of multi-unit nuclear power plants, Nuclear Engineering and Technology 53 (3) (2021) 967–973.
[18] Z. Cai, W.C. Xie, M.D. Pandey, S.H. Ni, Determining seismic fragility of structures and components in nuclear power plants using multiple ground motion parameters—Part I: Methodology, Nucl. Eng. Des. 335 (2018) 195–201.
[19] K. Kostinakis, I.K. Fontara, A.M. Athanatopoulou, Scalar structure-specific ground motion intensity measures for assessing the seismic performance of structures: a review, J. Earthq. Eng. 22 (4) (2018) 630–665.
[20] W. Du, S. Long, C.L. Ning, An algorithm for selecting spatially correlated ground motions at multiple sites under scenario earthquakes, J. Earthq. Eng. (2019) 1–26.

[21] B. Xu, X. Wang, R. Pang, Y. Zhou, Influence of strong motion duration on the seismic performance of high CFRDs based on elastoplastic analysis, Soil Dynam. Earthq. Eng. 114 (2018) 438–447.
[22] E. Zengin, N.A. Abrahamson, S. Kunnath, Isolating the effect of ground-motion duration on structural damage and collapse of steel frame buildings, Earthq. Spectra 36 (2) (2020) 718–740.
[23] Y.S. Choun, J. Park, I.K. Choi, Choun, Effects of mechanical property variability in lead rubber bearings on the response of seismic isolation system for different ground motions, Nuclear Engineering and Technology 46 (5) (2014) 605–618.
[24] A. Ali, N.A. Hayah, D. Kim, S.G. Cho, Probabilistic seismic assessment of base-isolated NPPs subjected to strong ground motions of Tohoku earthquake, Nuclear Engineering and Technology 46 (5) (2014) 699–706.
[25] G. Wang, Y. Wang, W. Lu, P. Yan, W. Zhou, M. Chen, A general definition of integrated strong motion duration and its effect on seismic demands of concrete gravity dams, Eng. Struct. 125 (2016) 481–493.
[26] M. Raghunandan, A.B. Liel, Effect of ground motion duration on earthquake-induced structural collapse, Struct. Saf. 410 (2013) 119–133.
[27] A. Ali, N. Abu-Hayah, D.K. Kim, S.G. Cho, Design response spectra-compliant real and synthetic GMS for seismic analysis of seismically isolated nuclear reactor containment building, Nuclear Engineering and Technology 49 (4) (2017) 825–837.
[28] J. Fayaz, M. Medalla, F. Zareian, Sensitivity of the response of Box-Girder Seat-type bridges to the duration of ground motions arising from crustal and subduction earthquakes, Eng. Struct. 219 (2020) 110845.
[29] L. Lombardi, F. De Luca, J. Macdonald, Design of buildings through linear time-history analysis optimising ground motion selection: a case study for RC-MRFs, Eng. Struct. 192 (2019) 279–295.
[30] D.D. Nguyen, B. Thusa, T.S. Han, T.H. Lee, Identifying significant earthquake intensity measures for evaluating seismic damage and fragility of nuclear power plant structures, Nuclear Engineering and Technology 52 (1) (2020) 192–205.
[31] PEER (Pacific Earthquake Engineering Research Center), Strong Motion Database, 2020. https://ngawest2.berkeley.edu/site.
[32] NECIS, (National Earthquake Comprehensive Information System), 2019. http://necis.kma.go.kr.
[33] J.H. Song, J.H. Baik, S.K. Zee, S.Y. Park, S. Choi, B.D. Chung, W.P. Baek, Development of a high power three-loop nuclear power plant, Nucl. Eng. Des. 240 (10) (2010) 3621–3631.
[34] N.H. Lee, K.B. Song, Seismic capability evaluation of the prestressed/reinforced concrete containment, 1999, pp. 189–203. Yonggwang nuclear power plant Units 5 and 6, Nuclear engineering and design, 192, 2–3.
[35] I.K. Choi, S.M. Ahn, Y.S. Choun, Seismic fragility analysis of PSC containment building by nonlinear analysis, Journal of the Earthquake Engineering Society of Korea 10 (1) (2006) 63–74.
[36] I.K. Choi, Y.S. Choun, S.M. Ahn, J.M. Seo, Probabilistic seismic risk analysis of CANDU containment structure for near-fault earthquakes, Nucl. Eng. Des. 238 (6) (2008) 1382–1391.
[37] M.K. Kim, J. Park, Y.S. Choun, I.K. Choi, Seismic fragility analysis for steel fiber applicability assessment for containment structure of nuclear power plant, Journal of the Computational Structural Engineering Institute of Korea 25 (5) (2012) 381–388.
[38] Y.S. Choun, J. Park, Evaluation of seismic shear capacity of prestressed concrete containment vessels with fiber reinforcement, Nuclear Engineering and Technology 47 (6) (2015) 756–765.
[39] T.K. Mandal, S. Ghosh, N.N. Pujari, Seismic fragility analysis of a typical Indian PHWR containment: comparison of fragility models, Struct. Saf. 58 (2016) 11–19.
[40] J.B. Park, N.C. Park, S.J. Lee, Y.P. Park, Y.G. Choi, Seismic analysis of the APR1400 nuclear reactor system using a verified beam element model, Nucl. Eng. Des. 313 (2017) 108–117.
[41] P.Y. Yawson, D. Lombardi, Probabilistic seismic risk assessment of nuclear reactor in a hypothetical UK site, Soil Dynam. Earthq. Eng. 113 (2018) 278–285.
[42] Nuclear Regulatory Commission, Standard review plan for the review of safety analysis reports for nuclear power plants: LWR edition (NUREG-0800), Nuclear Regulatory Commission, 1987.
[43] M.D. Trifunac, A.G. Brady, A study on the duration of strong earthquake ground motion, Bull. Seismol. Soc. Am. 65 (3) (1975) 581–626.
[44] O.W. Nuttli, The Relation of Sustained Maximum Ground Acceleration and Velocity to Earthquake Intensity and Magnitude, US Army Engineer Waterways Experiment Station, 1979.
[45] J.C. Foschaar, J.W. Baker, G.G. Deierlein, Preliminary assessment of ground motion duration effects on structural collapse. Proceedings of the 15th World Conference on Earthquake Engineering, 2012.
[46] L. Al Atik, N. Abrahamson, An improved method for nonstationary spectral matching, Earthq. Spectra 26 (3) (2010) 601–617.
[47] R.P. Kennedy, M. Shinozuka, Recommended minimum power spectral density functions compatible with NRC regulatory guide 1.60 response spectrum 34 (1989). Recommendations for Resolution of Public Comments on USI A-40, Seismic Design Criteria.
[48] L.E. Cover, M.P. Bohn, R.D. Campbell, D.A. Wesley, Handbook of Nuclear Power Plant Seismic Fragilities, NUREG/CR-3558, Washington, DC, 1985. US Nuclear Regulatory Commission.
[49] T. Uchida, N. Ohmori, T. Takahashi, S. Watanabe, H. Abe, Y. Aoyagi, Behavior of Reinforced Concrete Containment Models under the Combined Action of Internal Pressure and Lateral Force, 1979.
[50] Y. Aoyagi, K. Yamada, An Experimental Approach to the Design of Network Reinforcement against In-Plane Shear in Reinforced Concrete Containments, 1979.
[51] Y. Ogaki, M. Kobayashi, T. Takeda, T. Yamaguchi, S. Yoshizaki, S. Sugano, Shear strength tests of prestressed concrete containment vessels. Structural Mechanics in Reactor Technology, 1981. J (a).
[52] M. Kato, S. Tamura, Y. Watanabe, T. Takeda, T. Nakayama, Y. Omote, Dynamic and Static Loading Tests on 1/30 Scale Model of Prestressed Concrete Containment Vessel, 1981. Structural mechanics in reactor technology, Vol. K (b).
[53] Y. Aoyagi, S. Ohmori, K. Yamada, Strength and deformational characteristics of orthogonally reinforced concrete containment models subjected to lateral forces. Structural Mechanics in Reactor Technology, 1981. J (a).
[54] R.P. Kennedy, S.A. Short, K.L. Merz, F.J. Tokarz, I.M. Idriss, M.S. Power, K. Sadigh, Engineering characterization of ground motion, Woodward-Clyde Consultants, Walnut Creek, CA (USA), 1984. Task I. Effects of characteristics of free-field motion on structural response, NUREG/CR-3805, Structural Mechanics Associates, Inc., Newport Beach, CA (USA).
[55] N.M. Newmark, W.J. Hall, Development of Criteria for Seismic Review of Selected Nuclear Power Plants, NUREG/CR-0098, 1978.
[56] S.L. Kramer, Geotechnical Earthquake Engineering, Pearson Education India, 1996.
[57] J.J. Bommer, P.J. Stafford, J.E. Alarcón, Empirical equations for the prediction of the significant, bracketed, and uniform duration of earthquake ground motion, Bull. Seismol. Soc. Am. 99 (6) (2009) 3217–3233.
[58] A. Arias, Measure of Earthquake Intensity, Massachusetts Institute of Technology, 1970.
[59] G.W. Housner, Measures of severity of earthquake ground shaking, Proc. U. S. Natl. Conf. Earthq. Eng. 6 (1975).
[60] Y.J. Park, A.H.S. Ang, Y.K. Wen, Seismic damage analysis of reinforced concrete buildings, J. Struct. Eng. 111 (4) (1985) 740–757.
[61] J.W. Reed, R.P. Kassawara, A criterion for determining exceedance of the operating basis earthquake, Nucl. Eng. Des. 123 (2–3) (1990) 387–396.
[62] G.W. Housner, Spectrum Intensities of Strong-Motion Earthquakes, 1952.
[63] O.W. Nuttli, State-of-the-art for Assessing Earthquake Hazards in the United States. Report 16, the Relation of Sustained Maximum Ground Acceleration and Velocity to Earthquake Intensity and Magnitude, 1979.
[64] S.K. Sarma, K.S. Yang, An evaluation of strong motion records and a new parameter A95, Earthq. Eng. Struct. Dynam. 15 (1) (1987) 119–132.